

D. Marathe<sup>2,4\*</sup>, S. Shelar<sup>1</sup>, S. Mahajan<sup>3</sup>, Z. Ahmad<sup>3</sup>, S. Gupta<sup>3</sup>, S. Kulkarni<sup>3</sup>, V. Juvekar<sup>2</sup>, A. Lele<sup>1</sup>

<sup>1</sup>CSIR-National Chemical Laboratory, Pune, India

<sup>2</sup>Indian Institute of Technology Bombay, India

<sup>3</sup>Reliance Industries Limited, Mumbai, India

<sup>4</sup>Maharashtra Institute of Technology, Pune, India

# Study of Rheology and Plug Assist Thermoforming of Linear and Branched PP Homopolymer and Impact Copolymer

*Polypropylene (PP) is one of the fastest growing thermoplastic polymers in the world, second only to polyethylene. This is primarily due to its excellent balance of physical and chemical properties at a lower cost. PP however possesses low melt strength on account of its linear structure and hence is not easily amenable to processing techniques that involve free surface stretching deformations like thermoforming, blow molding and extrusion film casting. One way to enhance the melt strength of PP is to incorporate long chain branches in its molecular architecture. The present study focuses on the impact of rheology of linear and branched PP on their thermoforming characteristics. Two grades each of linear and long chain branched (LCB) PP homopolymer and impact copolymer (ICP) were used. It was observed that the LCB-PP homopolymer and LCB-ICP showed higher flow activation energy, reduced value of loss tangent and nearly equal frequency dependence of storage and loss moduli in shear rheology. Also, a strong strain hardening behavior was displayed in extensional rheology by the LCB grades. Plug assist thermoforming experiments were carried out to assess the effect of long chain branching on surface strain and thickness distribution for axisymmetric cups of two draw ratios. Biaxial surface strain maps of the formed cups were quantified using Grid Strain Analysis (GSA). Thermoformed cups made from LCB-PP homopolymer and LCB-impact copolymer showed lower surface strain and overall higher thickness as compared to cups made from their linear counterparts, which is in accordance with what might be expected from their rheology.*

## 1 Introduction

Thermoforming is a popular industrial processing operation that is used to manufacture diverse range of components from simple food packaging trays to more complex products such

as refrigerator liners and automotive components. In thermoforming, an extruded polymer sheet or film is heated to a desired softening temperature and is formed into a mold with the assistance of either pressure or vacuum. Plug assist thermoforming (PAF) is an important variant of the process wherein a mechanically operated plug is used to pre-stretch the sheet prior to application of vacuum or pressure. Pre-stretching prior to forming ensures relatively uniform thickness distribution compared to only vacuum/pressure forming (Throne, 1997).

Like extrusion film blowing or blow molding, thermoforming is a complex combination of extensional deformation processes. It is essentially a free surface forming process where the polymer is subjected to rapid biaxial deformation as the heated sheet is drawn into the mold (O'Connor et al., 2008). Stretch rates experienced during thermoforming are between 1 and 20 s<sup>-1</sup> (Martin et al., 2005). During PAF when the sheet is mechanically pre-stretched with a plug, it undergoes predominantly uniaxial extension between its anchor points. The sheet experiences constrained orientation in this case. In the next step during forming with a pressure differential, the sheet undergoes unconstrained deformation, which is essentially uniformly biaxial in the center of the sheet and uniaxial at the clamped edges (Throne, 1996).

For a component made by thermoforming, the two dimensional sheet has to cover a finite amount of surface. When the sheet is heated and forced into the cavity, it must stretch to conform to the shape of the cavity. As the sheet stretches, it thins out. Local design features on the part may cause the sheet to thin in an uneven manner. Therefore, at the forming temperature, the polymer should possess the right balance of viscous and elastic properties. It should be viscous enough to flow and duplicate all the intricate features of the mold but at the same time be elastic enough to sustain the stresses experienced during biaxial deformation and maintain its structural integrity. Amorphous materials like High Impact Polystyrene (HIPS), Acrylonitrile Butadiene Styrene (ABS) and polystyrene (PS) are thermoformed in the rubbery region between glass transition temperature and the temperature where the material modulus is around 1 MPa. In this wide temperature window, the sheets have the right balance of viscous and elastic properties

\* Mail address: Deepti Marathe, Maharashtra Institute of Technology, Survey No.124, Paud Road, Pune, India  
E-mail: deepti.marathe@mitpune.edu.in

as well as high flow activation energy and strain hardening, which make them well suited to thermoforming (Barroso et al., 2003).

Semi-crystalline polymers like polypropylene (PP) and its co-polymers have low melt strength and low elasticity due to their linear macromolecular architecture (Maier and Calfut, 2002). Only a narrow temperature window above the melting temperature is available for thermoforming since a steep drop in modulus above the melting temperature poses a challenge for sustaining the stresses induced during biaxial deformations in thermoforming. Further, low melt strength results in excessive sagging of the sheet prior to forming, which leads to uneven deformation and uneven thickness distribution in the product (Lau et al., 2000). Though Solid Phase Pressure Forming (SPPF) below melting temperature between 155 to 165 °C is possible for PP, it is not as popular as melt phase forming since the high pressure required for forming results in the presence of residual stresses in the formed components (Tripathi, 2002).

PP can be made more amenable to thermoforming by enhancing its melt strength and melt elasticity. Successful thermoforming can lead to opening up of new markets for PP. Therefore, in recent years, there is growing interest in developing High Melt Strength (HMS) grades of PP (Graebing, 2002). There are numerous ways of increasing the melt strength of PP. They are: (i) increasing the weight average molecular weight, (ii) broadening the molecular weight distribution particularly by creating bimodal resins containing considerable fraction of high molecular weight chains, (iii) blending PP with polymers such as low density polyethylene (LDPE), and (iv) introducing long chain branching (LCB) on the backbone of PP (Borsig et al., 1989; DeNicola, 1990; Guo et al., 2014; Wang et al., 1996). There are however important concerns with each of these options. Increasing the molecular weight affects processability, creation of bimodal PP is not easy to implement in many conventional reactor technologies, and immiscibility of LDPE and PP adversely affect properties such as transparency. Introduction of long chain branching on PP chains is perhaps the most attractive option since long chain branching is known to significantly enhance extensional resistance of an entangled melt (Chikhalikar et al., 2015). The length necessary for a branch to behave as a “rheologically long” chain branch is  $\alpha M_e$ , where  $\alpha > 10$  and  $M_e$  is molecular weight between entanglements.

Long chain branched polypropylene (LCB PP) can be made by “in-reactor” as well as “post-reactor” treatment of polypropylene. In-reactor methods include synthesis of LCB PP using metallocene or constrained geometry catalyst in presence of macromonomer and non-conjugated diene comonomer (Shino et al., 1999; Arnold et al., 2002). Post-reactor treatments include solid state electron beam irradiation (e.g., Scheve, 1990); reactive extrusion in presence of peroxide, multifunctional monomers and coagents in melt state (e.g., Wang et al., 1996); and blending of linear PP with LCB-PP/LDPE (e.g., Borsig et al., 1989). Because of its relative ease of implementation on commercial scale, reactive extrusion is the most popular post-reactor process to make LCB-PP. Its main advantages include very short reaction times, little or no use of solvents, simple product isolation step and relatively low infrastructure costs as compared to other methods (Moad, 1999).

Reactive extrusion of PP is commercially practiced to manufacture controlled rheology grades of PP to achieve faster injection molding cycles (Tzoganakis 1988; Tripathi, 2002), for functionalization of PP (Bettini, 2002; Li, 2003) and crosslinking of PP (Coiai, 2004; Kim, 1993). The process involves extrusion of PP in presence of organic peroxides and/or multifunctional comonomers and/or coagents in a twin-screw extruder or a batch mixer. Various reactions occurring during reactive extrusion of PP in presence of peroxide include degradation by  $\beta$ -scission of the macroradicals and crosslinking by recombination of macroradicals (Chodak, 1982). Wang and co-workers (1996) studied reactive extrusion of PP in presence of pentaerythritol triacrylate (PETA) and 2,5-dimethyl-2,5-(*t*-butylperoxy) hexane peroxide (trade name Lupersol 101, Sigma Aldrich, Beijing, PRC). Measurements of shear viscosity and MFI of the modified PPs indicated an enhancement of viscosity, and therefore, an increase in molecular weight. It was observed that the amount of macrogel in the modified PP increased with increasing PETA and peroxide concentrations. Legendijk and co-authors (2001) carried out reactive extrusion in the presence of selected organic peroxydicarbonates (PODIC). This was shown to result in the formation of long chain branching as confirmed by high temperature size exclusion chromatography combined with on-line intrinsic viscosity measurements. All branched samples showed distinct strain hardening in elongational rheology, lower MFI, increased extrudate swelling and improvement of melt strength by up to a factor of two. They concluded that PODIC with non-linear or large linear alkyl groups resulted in modified PP with the highest degree of branching and the fastest strain hardening. Graebing (2002) obtained LCB PP using reactive extrusion in the presence of peroxide, 2,5-dimethyl-2,5-di(*tert*-butyl peroxy)hexane, a polyfunctional acrylate monomer, trimethylol propane triacrylate (TMPTA), and various sulphide compounds as coagents. Long chain branched structure was obtained in presence of the coagent, thiuram disulfide, and the same was confirmed by the increase in elastic modulus and terminal relaxation time. It was observed that the dithiocarbamate radicals can be reacted with the macroradical PP in a reversible reaction. These radicals induce a decrease in the instantaneous concentration of free radicals and thus limit the  $\beta$ -scission, which favors the reaction between TMPTA and macroradical PP thereby leading to increase in the efficiency of branching. Parent et al. (2008) carried out reactive extrusion of PP in the presence of triallyl trimellate (TAM). They observed that the graft modification of PP gave bimodal molecular weight and branching distributions. Precipitation polymerization of TAM can proceed concurrently with branching to produce a low yield of crosslinked, TAM-rich nano-particles. In a following paper, Parent et al. (2009) carried out reactive extrusion of PP in presence of trifunctional coagent such as TAM, trimethylolpropane triacrylate (TMPTA) and triallyl phosphate (TAP). Branching was confirmed by carrying out shear and extensional rheological measurements.

Mabrouk et al. (2009) adopted single step and two step methodologies to make LCB PP by reactive extrusion. The single step process involved radical-mediated addition of PP to triallyl phosphate, while the two-step process involved sequential addition of PP to vinyltriethoxysilane followed by moisture-curing. The two-step approach was seen to improve low-

frequency shear viscosity and extensional strain hardening characteristics. Su and coworkers (2010) made LCB PP by reactive extrusion in presence of various peroxides and a poly-functional monomer 1,6 hexanediol diarylate. Modified samples showed higher melt strength and lower MFI. It was observed that branching level could be controlled by the structure of the peroxide. Peroxides with lower decomposition temperature and stable radicals after decomposition led to higher branching levels and hence melt strength.

Park and Chung (1997) studied cell nucleation in linear and LCB PP using carbon dioxide and isopentane as foaming agents. They observed that branched PP gave a closed cell structure. On the other hand, cells were interconnected in the foam made from linear PP. Melt strength and elasticity of the branched PPs determined the cell morphology. Spitael and Macosko (2004) studied the effect of long chain branching on foamability. A linear PP and two grades of LCB PP were foamed on a twin-screw extruder foaming line with carbon dioxide as blowing agent. Branched polymers exhibited strain hardening which lead to stabilization of foam. Blends of linear and LCB PP showed better cell concentration suggesting that long chain branching improved foamability.

Gotsis et al. (2004) modified linear PP by reactive extrusion with peroxydicarbonates in a twin-screw extruder. Melt strength, elasticity and strain hardening were observed to increase with increase in the number of long chain branches on the main chain. The processability in foaming and thermoforming processes was found to improve with branching but showed an optimum, beyond which higher degrees of long chain branching did not help.

Lau et al. (1998) measured the melt strength of linear PP homopolymer and copolymer and LCB PP homopolymer to assess the sagging resistance for thermoforming applications. They observed that the LCB PP grade had significantly higher melt strength than linear PP indicating that the LCB PP would have improved sag resistance. Lau et al. (2000) compared the isothermal sagging resistance for different grades of conventional and HMS PP. The HMS PP grades showed higher zero shear viscosity, lower loss tangent, lower frequency dependence of storage modulus and higher melt strength. Results of sagging resistance measured at 190 °C correlated well with the rheological properties. The HMS PP grade showed higher sagging resistance than the linear PP.

Munstedt et al. (2006) studied the extensional rheological properties and thermoforming behavior of linear PP copolymer and LCB PP. They observed that the LCB PP showed strain hardening behavior for all the shear rates in the elongational experiments. Beakers thermoformed from the linear PP showed pronounced minimum in thickness distribution. LCB PP showed better homogeneity in thickness distribution. It was concluded that the better homogeneity in the thickness is due to the long chain branching. Gezaz and co-authors (2006) prepared ternary blends of PP/HDPE/EPDM and their thermoformability was investigated by hot tensile and rheological tests. Blends had higher elasticity and sag resistance as compared to neat PP. The results confirmed that blending with HDPE and EPDM improved the thermoformability of PP.

Chikhalikar et al. (2015) studied extrusion film casting for linear and LCB PP homopolymers. They observed that LCB PP samples displayed more significant reduction in necking

than linear PP at comparable draw ratios. Necking was higher closer to the die exit but decreased as the film approached the chill rolls. Kumar et al. (2014) studied thermoforming of linear and long chain branched PP. It was observed that double sided heating gave good part conformance for drape forming of the 5 mm thick sheets. The LCB PP was found to have lower crystallinity and lower sag. The component formed with LCB PP gave a more uniform thickness distribution as compared to the linear PP. They also observed that at higher draw depths, effect of draft angle on wall thickness distribution was significant as compared to lower draw depths. Irrespective of material and draw depth, generous corner radii gave stronger corners.

The literature review above primarily focuses on development of technologies for making of LCB PP and its molecular, rheological and thermal characterization. Studies showing the effect of long chain branching on thermoforming are fewer. Only two groups (Kumar et al., 2014; Munstedt et al., 2006) have compared the thermoforming behavior of linear and long chain branched PP by forming products and comparing their thickness distribution. However, none have so far studied the surface strain distribution of linear and branched PP. Establishing the link between surface strain distribution and thickness distribution enables improved understanding of the deformation occurring during thermoforming. Also, there are no studies on understanding the effects of plugging and vacuum forming stages separately on deformation of linear and branched PP.

The present work focusses on plug assist forming of axisymmetric cups of two different draw ratios using linear and long chain branched PP. Detailed comparison of sagging of the sheets before PAF as well as the thickness distribution and surface strain distribution in the formed components is made. The results of sagging for the linear and LCB PP are correlated with their rheological properties, and effects of sagging on strain distribution and thickness distribution are discussed. Thus, the study illustrates the effects of macromolecular architecture on PAF. The work presented here is organized as follows. Materials and various experimental details related to rheological measurements, independent sagging experiments and forming experiments are described in section 2. The main results of the work on sagging and forming are discussed in section 3. Section 4 summarizes the conclusions of this work.

## 2 Materials and Methods

### 2.1 Materials

A commercial linear impact copolymer of polypropylene, ICP (grade Repol C015EG, MFI 1.5 g/10 min, Reliance Industries Ltd., Mumbai, India) and a commercial high melt strength grade of impact copolymer of polypropylene, ICP-C (MFI 0.6 g/10 min, grade D114, Dow Chemicals, Midland, USA) were used in this study. Along with these copolymers, two grades of PP homopolymer, linear PP 3H1 (MFI 3.32 g/10 min, Reliance Industries Ltd.) and a modified grade having long chain branching 3H4 (MFI 1.5 g/10 min) were also used in this study. As reported in a previous work (Chikhalikar et al., 2015), LCB containing 3H4 was prepared by premixing 3H1 with 5000 ppm of hexadecoxycarbonyloxy hexadecyl carbonate (Perkadox 24L, Akzo No-

bel, Amsterdam, The Netherlands), 500 ppm of primary antioxidant Irganox-1010 (BASF SE, Ludwigshafen, Germany), 1000 ppm of secondary antioxidant Irgafos 168 (BASF SE) and 250 ppm of co-agent zinc diethyldithiocarbamate (Mercur ZDC, Merchem Ltd., Kochi, India) in a high-speed homogenizer followed by compounding it in a 30 mm co-rotating twin screw compounder (Omega 30, Steer, Bengaluru, India). The compounder had a mixing screw configuration with  $L/D = 40$ , and the temperature in the various zones of the twin screw extruder was varied from  $160^{\circ}\text{C}$  to  $220^{\circ}\text{C}$ . Details of molecular characterization, extrudate swell, MFI, melt strength, crystallization temperature  $T_c$  and melt temperature  $T_m$  of these grades have been reported earlier (Chikhalikar et al., 2015) and are summarized below in Table 1.

## 2.2 Rheology

Linear viscoelastic properties of all the PPs were determined by carrying out Small Amplitude Oscillatory Shear (SAOS) tests on a strain-controlled rheometer (ARES, TA Instruments, New Castle, USA) using parallel plate geometry (25 mm diameter plates, 1 mm gap). SAOS tests were performed over a temperature range of  $170^{\circ}\text{C}$  to  $230^{\circ}\text{C}$  and over a frequency range of 0.01 to 100 rad/s. The dynamic moduli,  $G'$  and  $G''$ , and the loss tangent  $\tan \delta$  were determined as functions of the frequency. The dynamic rheology data at various temperatures were shifted horizontally along the frequency axis to a reference temperature of  $170^{\circ}\text{C}$ . From the master curves so obtained a discrete 8-mode relaxation spectrum  $\{\lambda_i, G_i\}$  and WLF shift factors were derived. Uniaxial extensional viscosity data was generated from step elongation experiments. These experiments were carried out using the SER Universal Testing Platform from Xpansion Instruments, which works on the rheometer and records the tensile stress growth coefficient as a function of time at different stretch rates. Tensile stress growth was measured at stretch rates varying from 0.1 to  $10\text{ s}^{-1}$  at  $170^{\circ}\text{C}$ . Though thermoforming was carried out at  $190^{\circ}\text{C}$ , the extensional experiments were not performed at the same temperature since the samples tend to sag considerably before being subjected to extension. Sagging affects the extensional data and these effects cannot be corrected. Since sagging was minimal at  $170^{\circ}\text{C}$ , extensional tests were easier to perform at this temperature and the data amenable to clear analysis. Moreover, as the polymers obeyed time-temperature superposition (TTS) principle, it is possible to predict extensional viscosity of the samples at the thermoforming temperature of  $190^{\circ}\text{C}$  from the  $170^{\circ}\text{C}$  data.

## 2.3 Sagging

In thermoforming, the clamped sheet sags during the heating stage just before forming. Strain rates are very low, typically around  $0.01\text{ s}^{-1}$  (Giacomin, 2010). The extent of sagging is determined by the material rheology. Independent sagging experiments were performed to highlight the effect of long chain branching. The experimental fixture used for sag studies consisted of a couple of circular steel rings, 200 mm in diameter and 5 mm thick between which PP sheets were clamped. The rings were supported by four adjustable bolts and nuts. 3 mm thick square sheets of PP of dimensions  $210\text{ mm} \times 210\text{ mm}$  with corners cut to enable visual observations of sag were used for the experiments (Fig. 1). The fixture was placed inside an air circulating oven having a glass window for observation. The fixture was preheated inside the oven to the experimental temperature of  $190^{\circ}\text{C}$ . After thermal equilibration, the sheets were clamped into the fixture and placed in the oven. Sheet temperature was recorded on the top surface with a RTD. After a soak time of about one minute during which the sheets reached the set temperature, images of sagging were captured at 25 frames per second for 260 s. These experiments were repeated for 5 sheets of each PP material. Sag in the initial stages till 10 mm depth could not be recorded as the view was obstructed by the fixture. Zero time was chosen at the moment the sheet became visible below the fixture. The maximum sag

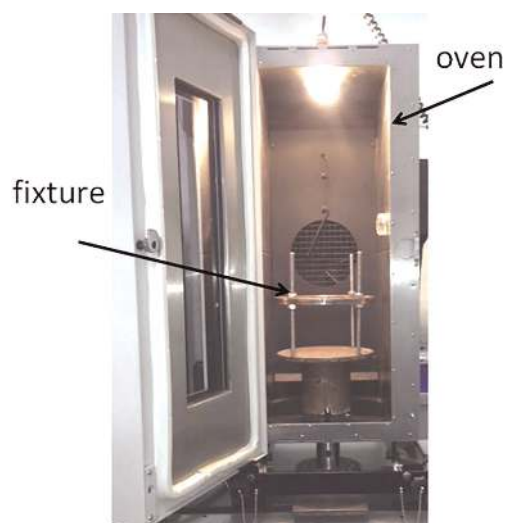


Fig. 1. Experimental set-up for sagging

Sr. No.	Sample	Description	MFI g/10 min	$T_c$ $^{\circ}\text{C}$	$T_m$ $^{\circ}\text{C}$	Dieswell %
1	3H1	linear homopolymer	3.3	118	164	36
2	3H4	branched homopolymer	1.5	129	164	102
3	ICP	linear PP impact copolymer	1.5	112	163	9
4	ICP-C	branched PP impact copolymer	0.6	125	165	80

Table 1. Materials

time of 260 s was chosen such that the sheet that sagged the most did not touch the oven base. A commercial CCD camera (Uniq Vision Inc., Santa Clara, USA, model UM201) with a zoom lens (Pentax, Tokyo, Japan, model C61215TH of 12 mm focal length and C-mount) was used to record the sag images. The CCD camera was connected to a PC equipped with a frame grabber card (EPIX Inc., Buffalo Grove, USA, model SV5). The sequence of images captured by the CCD camera during sheet sagging were analyzed with image analysis software Image J.

#### 2.4 Plug Assisted Forming

3 mm thick extruded sheets of ICP, ICP-C, 3H1 and 3H4 were obtained from Arihant Goldplast Ltd., Mumbai, India. These were used in plug assist vacuum forming experiments, which were performed using a single stage thermoforming machine (model SPM-55, Wonderpack, Nashik, India). Two axisymmetric container shaped aluminum molds of two different draw ratios were used in the forming experiments. The dimensions and shapes of the molds and their corresponding plugs are shown in Fig. 2. Cartridge heaters were used to heat the plug, and its surface temperature was controlled using a RTD coupled with a PID 313 temperature controller. The plug temperature during forming was set at 100 °C. PP sheets were heated using a bank of movable infrared heaters from the top and the bottom. Temperature of the top surface was continuously monitored using an infrared temperature sensor. The bottom surface temperature was separately measured using a hand-held IR sensor immediately after the heaters were retracted and was found to be slightly higher than the top surface temperature. This was caused by sagging of the sheet, which made it approach the bottom heater.

In a typical PAF experiment, the sheet was inserted in between the heaters and heated for about 140 s till the sheet temperature reached the forming temperature of 190 °C. The sheet was then taken to the molding station where it was clamped and the plug was rammed down at the pre-set speed of

200 mm/s. After the maximum travel of the plug, the final forming was done by application of vacuum (40 kPa). Some experiments were done by demolding the components after plug forming but before the final stage of vacuum forming. These experiments are called as “plug-only” forming. In “Plug-only” experiments, forming was carried without the cavity. Forming was stopped immediately after the plug travel is complete. The partially formed cups were cooled using an air blower for one minute till the temperature reached around 70 °C.

Prior to forming, a grid pattern of 5 mm diameter circles was screen-printed on the sheets. The spatial distribution of thickness of the formed cups was quantified by measuring the thickness at the center of each grid circle using a hand-held ultra-sonic thickness gauge having a maximum error of  $\pm 2$  microns over the measurement range of 30 microns to 3 mm. Thickness measurements were carried out along 3 arcs separated by 120°. Each arc traces the surface of the molded container starting from the top to the center of its base at the bottom (see Fig. 2A). Average values of thicknesses measured for 4 components are reported here.

Two orthogonal diameters were also printed on every circle of the grid pattern. The diameters were oriented along the length and breadth of the sheet. Upon forming, the grid circles deformed into ellipses or larger circles depending on the nature and magnitude of strain experienced locally by the sheet (Fig. 3). Consequently, the two diameters of the grid circles also deformed into two axes of the corresponding ellipses. The lengths of these axes were used to quantify the local surface strains of the thermoformed component using the technique of Grid Strain Analysis (GSA) (Sowerby et al., 1982; Schaeffler, 2006). Surface strains are defined as the absolute difference between the diameter of the original circles and the lengths of the axes of the corresponding ellipses formed after deformation, normalized by the diameter of the original circles (5 mm). Thus, local surface strains can be defined along the two directions of the axes of the ellipse. The results described in this work are based on the choice of two specific directions: Direction-2 (axial direction) is along an arc that spans between

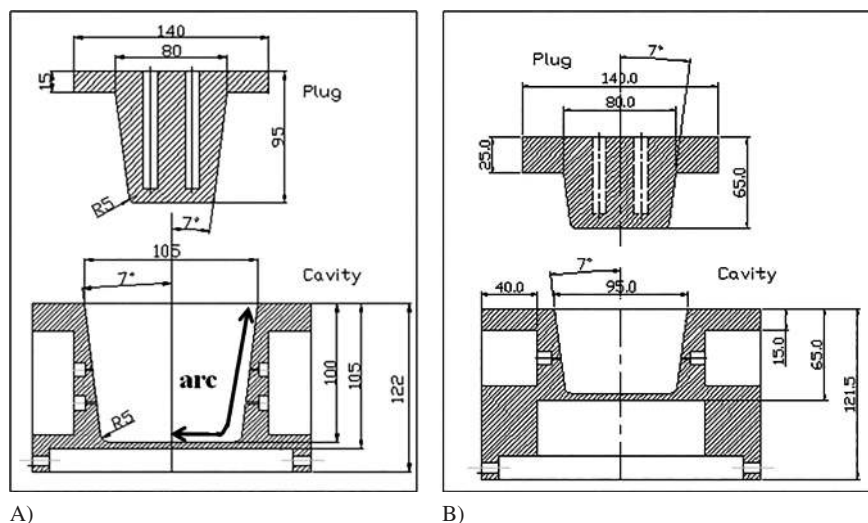


Fig. 2. Design of cavity and plug assist for A) 100 mm and B) 60 mm

the clamped sheet and center of the base of the formed cup, while direction-1 is the circumferential direction (Fig. 2). We also define area strain as

$$\text{area strain} = \frac{\text{area of ellipse} - \text{area of initial circle}}{\text{area of initial circle}}$$

The dimensions of the two axes of each ellipse were measured using a Co-ordinate Measuring Machine (CMM) (Cordimeasure E01-01, Accurate, Pune, India). An electronic touch trigger probe (Reinshaw, Gloucestershire, UK) comprising a 1 mm diameter spring loaded steel ball stylus controlled by a hand box with a joystick was used for the measurements. For any given ellipse, the dimensions of its axes (oriented along axis-1 and axis-2) were measured by positioning the probe on several points along the axes and adding the (small) linear distance between these points. The surface strains along the two axes were calculated from the measured dimensions. Besides the surface strains, we have also used the aspect ratio of the ellipses as a measure of the local deformation. The aspect ratio is defined here as the ratio of the lengths of axis-1 and axis-2 of the ellipses.

The sheets sagged to varying extents before forming. Sagging affects the thickness and surface strain distribution of the formed component. In order to get some estimate of sag prior to forming, the sheet deformation was captured with a camera having a speed of 30 frames per second. During the forming process, it took a minimum of 4 s for the plug to touch the sheet after the heaters move back. Sagging of the sheet during this time was recorded and quantified by image analysis.

### 3 Results and Discussion

#### 3.1 Rheology

Figure 4 shows master curves obtained at the reference temperature of 170 °C applying the time temperature superposition

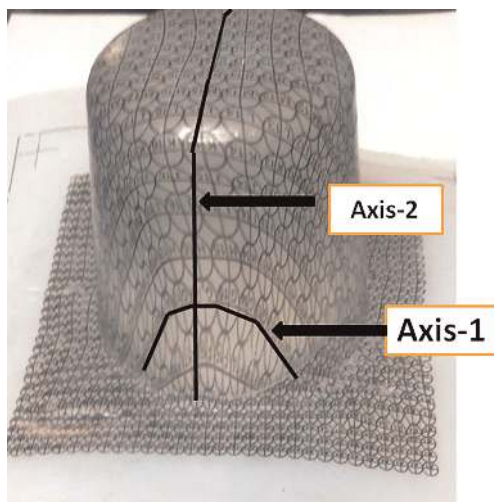


Fig. 3. Formed component from ICP-C showing deformed circles

(TTS) to SAOS data. Figures 4A and B show TTS for linear PP copolymer (ICP) and homopolymer PP (3H1). The slopes in the low frequency region for  $G''$  and  $G'$  are 1 and 1.3 respectively. The value of slope  $< 2$  for  $G'$  is due to the broad molecular weight distribution of the PP samples indicating that the terminal regime may be expected at still lower frequencies. In TTS master curves for branched polymers ICP-C and 3H4 (Figs. 4C and D),  $G'$  showed still weaker frequency dependence, and in fact  $G'$  and  $G''$  are almost parallel in the low frequency region. Branching adds slower relaxation modes, which are absent in linear polymers and hence the terminal region is expected at even lower frequencies (Kasehagen et al., 1996).

Correspondingly, it can be seen from Figs. 4E and F that ICP-C and 3H4 show a plateau in the loss tangent in the low frequency regime, and the values of loss tangent are lower than those of linear polymers. Also, for the branched samples ICP-C and 3H4, the flow activation energies are higher and the characteristic relaxation times as measured from the crossover frequencies are higher than the linear counterparts (Table 2). These observations are in agreement with those reported in previous studies (Borsig et al., 2007; Graebing, 2002; Adams et al., 2000).

Figures 5A and C show the extensional rheology of the linear copolymer (ICP) and homopolymer (3H1). No strain hardening was observed and the behavior is consistent with the linear viscoelastic regime over the entire range of strain rates considered for the experimental data. This is expected for linear polymers (Hingmann, 1994; Kurzbeck, 1999). On the other hand, as seen in Figs. 5B and D, both the branched polymers ICP-C and 3H4 show deviation from their linear viscoelastic behavior at large strains. Strain hardening is observed in both materials at all strain rates as the extensional viscosity rises above the linear viscoelastic envelope. Strain hardening response is observed when the polymer chains are stretched above their equilibrium contour length. This happens if the stretch relaxation time is higher than the inverse of the imposed stretch rate. Since for linear chains of moderate molecular weights the stretch relaxation time is typically small, therefore strain hardening is not easily observed. However, branched polymers undergo hierarchical relaxation processes where the branches relax first followed by the backbone. Because of this, the stretch times of the backbone are substantially higher. Hence long chain branched polymers often show an increased tendency to strain harden. The increased resistance of branched PP grades to elongational deformation is also reflected in their melt strength. The melt strength values are reproduced in Table 2. As can be seen, ICP-C has the highest melt strength. 3H4 has almost double the melt strength of 3H1. In summary, the shear and extensional rheology results clearly indicate higher melt strength and elasticity for branched polymers.

#### 3.2 Sagging

Figure 6 shows time dependent sagging of half width of an ICP sheet at 190 °C. The sag profiles are flat and close together initially (up to 200 s) beyond which they separate at a faster rate. The sag increases gradually till 200 s after which it accelerates.

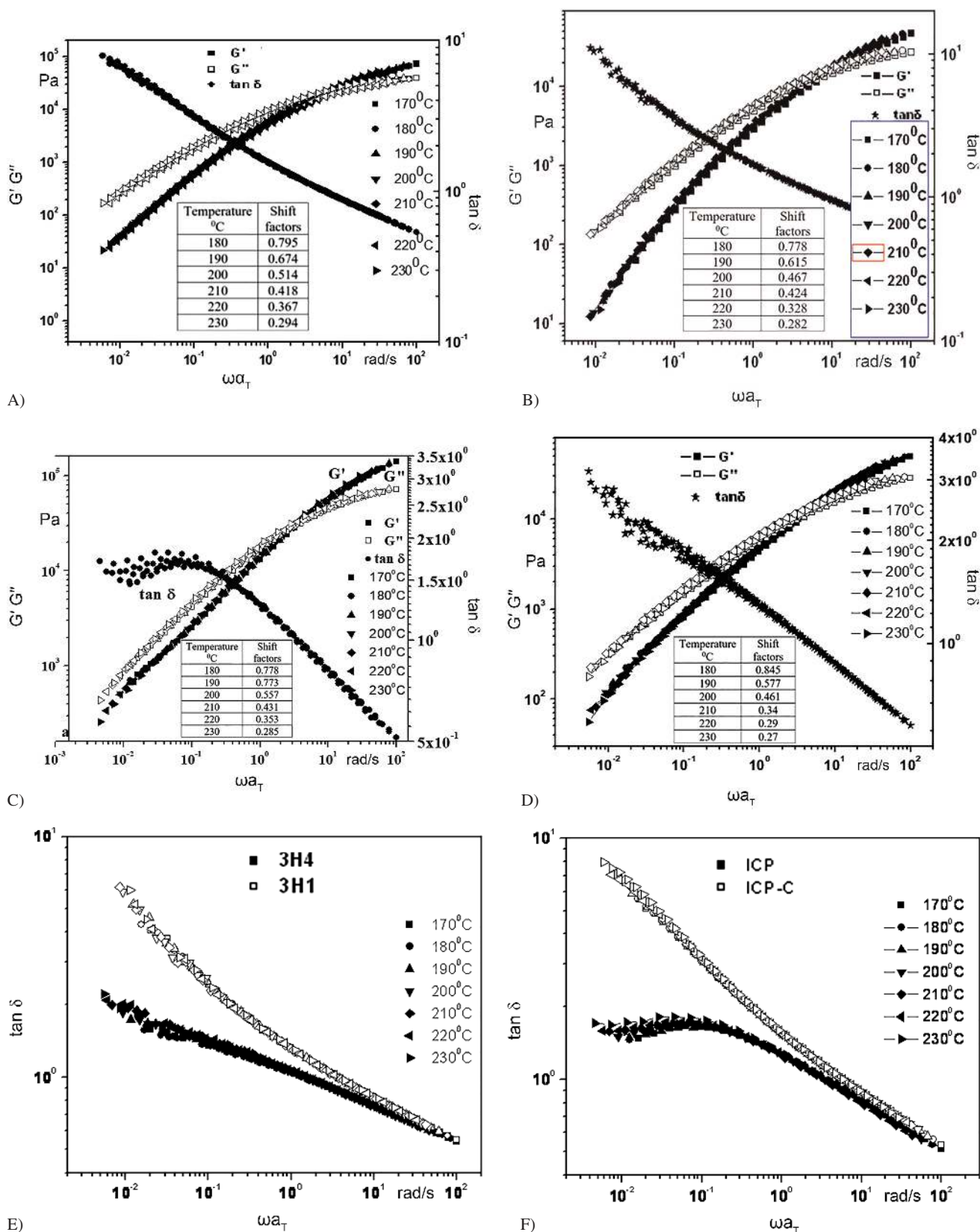


Fig. 4. Time temperature superposition master curves at  $T_{ref} = 170^{\circ}\text{C}$  for A) ICP, B) ICP-C, C) 3H1, D) 3H4. The numbers in the legend refer to temperature in  $^{\circ}\text{C}$  at which oscillatory raw data was obtained. Loss tangent comparison for E) homopolymers and F) copolymers. The numbers in the legend refer to temperature in  $^{\circ}\text{C}$  at which oscillatory raw data was obtained

These results are similar to those obtained by Lau et al. (2000). Branched ICP-C does not sag at all. Higher ZSV (or equivalently, higher low-frequency complex viscosity) and high melt strength (or equivalently, higher low-frequency elastic modulus) due to presence of branching leads to no sag for ICP-C.

Figure 7 shows sagging of half width of the 3H1 sheet with time at 190 °C. The nature of the curves is similar to ICP with the curves flatter and close to each other up to 170 s beyond which they separate more rapidly. Figure 8 shows sag for 3H4 at 190 °C. A negative sag or reversion is observed in this case

Material	Activation energy kJ/mol	Cross-over frequency at 170 °C	Relaxation time s	Melt strength mN	Zero shear viscosity at 190 °C from SAOS Pa s	Zero shear viscosity at 200 °C from SAOS Pa s
ICP	37	5.88	0.17	128	17,761	13,923
ICP-C	39	3.41	0.29	310	74,400	57,900
3H1	39	8.5	0.12	97	8,878	7,211
3H4	43	4.7	0.21	200	19,565	16,284

Table 2. Rheological properties

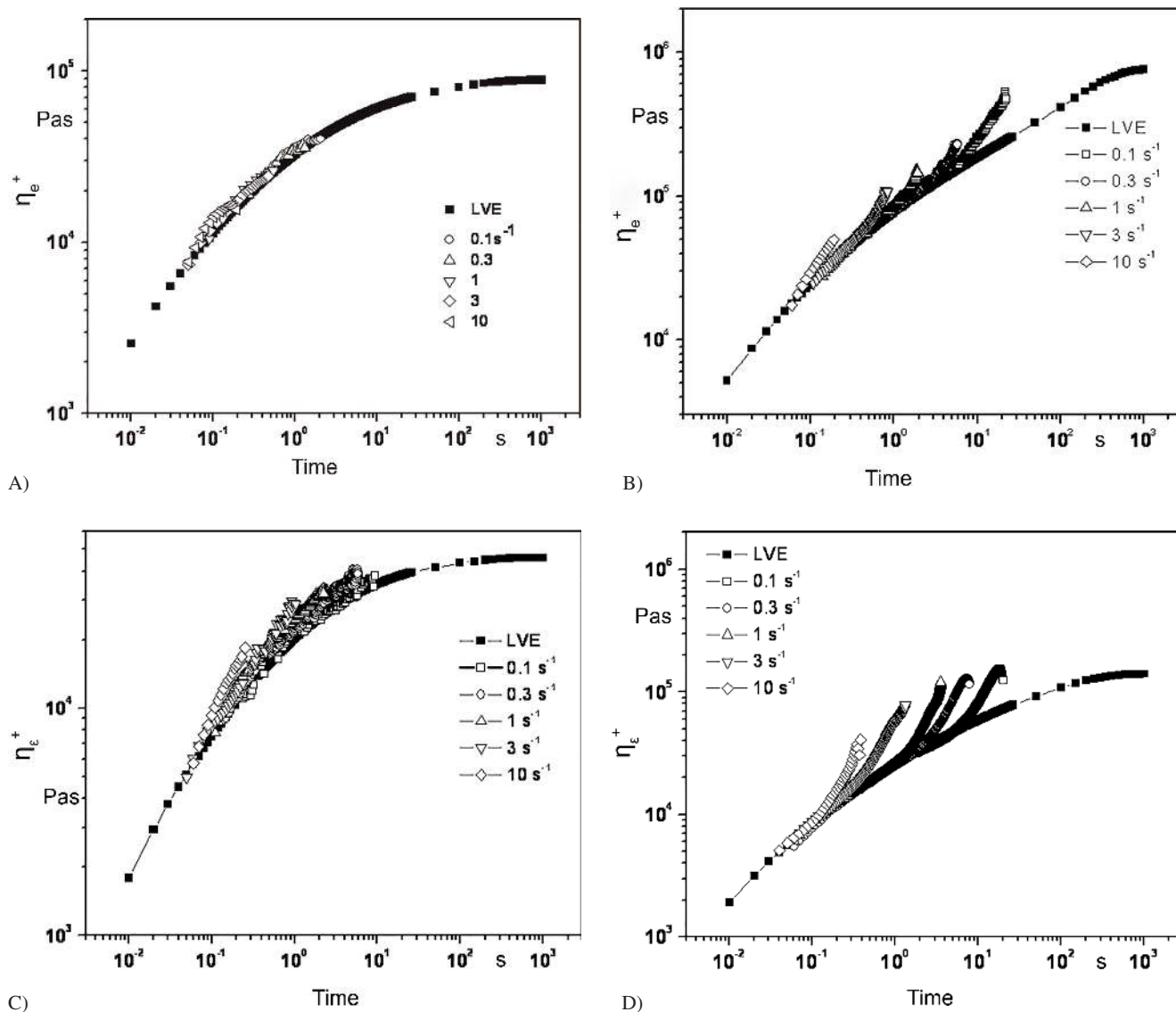


Fig. 5. Extensional flow data with KBKZ model fit at 170 °C for A) ICP, B) ICP-C, C) 3H1, D)3H4. The numbers in the legend refer to various extensional rates used during experiments



in the initial time period of < 50 s. The sheet instead of sagging downwards, bulges progressively upward. Giacomini et al. (2010) have reported such a negative bulge or reversion or sheet upswing for linear PP. This phenomenon can be attrib-

uted to residual stresses from sheet extrusion. As seen in Fig. 8, after initial reversion, the sheet progressively sags downwards. The sheet movement could not be captured by the camera during the transition between reversion and downward movement as the fixture obstructed the view.

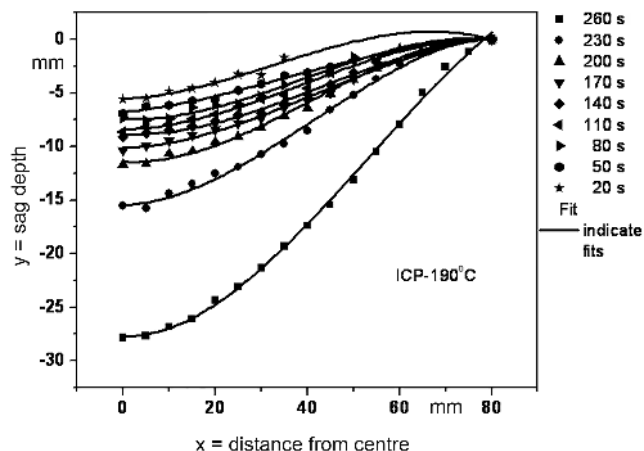


Fig. 6. Sag depths for IPC at 190°C

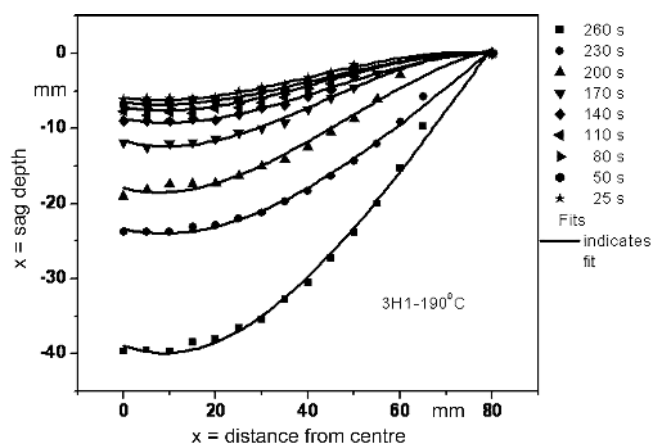


Fig. 7. Sag depths for 3H1 at 190°C

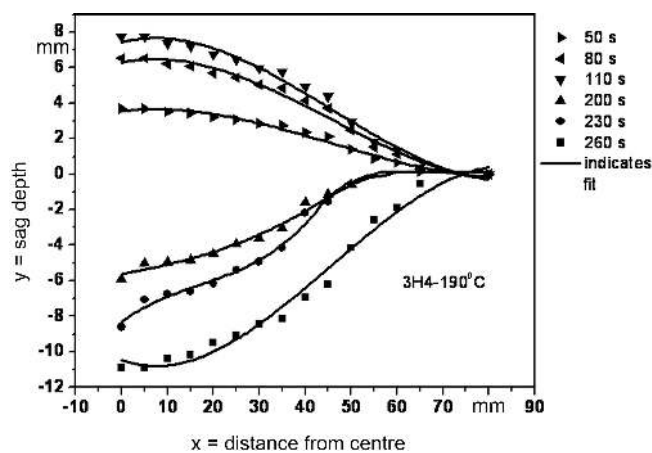


Fig. 8. Sag depths along arc length for 3H4 at 190°C

### 3.3 Plug Assisted Forming

We will now look at the results of thickness and surface strain distributions of thermoformed components made from the linear and branched PP samples. While both tool geometry and material characteristics affect the surface strain and thickness distributions, the sag prior to forming has a more subtle effect. The sheet begins to sag during the heating stage and continues to sag as the heaters move back. The total sag time is estimated to be the heating time plus another 4 s, which is the time it takes for the plug to touch the sheet. The extent of sagging of sheet during this time was experimentally determined as already explained earlier. Additionally, we have seen from the independent isothermal sag experiments that the branched PP sags to significantly lesser extent than the linear PP. The effects of these differences are described below.

Figures 9A, B show the sagged profile of the linear PP sheets – ICP and 3H1, at the instant when the plug touches the sheet in the two molds of different draw ratios. The distance between the two vertical lines in Figs. 9A, B represents the half widths of the plugs, which are respectively 20 mm for the 40 mm deep plug, and 30 mm for the 80 mm deep plug. The horizontal line in Figs. 9A, B shows the total travel for the two plugs, which is equal to the plug depth. As can be seen from Fig. 9A for the 60 mm deep cup, the plug base will not touch the ICP sheet for an initial 20 mm travel. For the remaining 20 mm travel of the plug, the sheet will come in contact with the plug base. In case of the 100 mm deep cup (Fig. 9B), though the plug base will not be in contact with the sheet for an initial travel of 30 mm, it will come in contact with the sheet for the major part of the remaining travel. Thus, it is seen that for the 60 mm deep cavity the deformations of the ICP and 3H1 sheets are caused by sag and plug forming. In contrast with the 100 mm deep cavity, the plug movement dominates the deformations of the ICP and 3H1 sheets.

Contrarily to the linear PP sheets, the branched PP sheets showed little sagging. While ICP-C did not sag at all, the sag of 3H4 was finite but small and was hindered from view by the clamping frame of the machine. Hence it was not possible to record and quantify the sags of these two polymers. Because of the low sag, the plug base is expected to be in complete contact with the sheets of branched PPs for the two draw depths, and thus the deformation of the sheet is mostly due to plug motion rather than by sag. In summary, the mechanism of plug assist forming for linear and branched PPs will be determined by sagging and plug movement depending on the draw ratio and the rheology of the material.

In the following discussions we will analyze the surface strain distributions and thickness distributions for “plug-only” and PAF experiments for the two pairs of linear and branched PP materials and for the two containers of different draw ratios. Comparison between “plug-only” and PAF data helps in understanding the role of pre-stretching caused by plug motion.

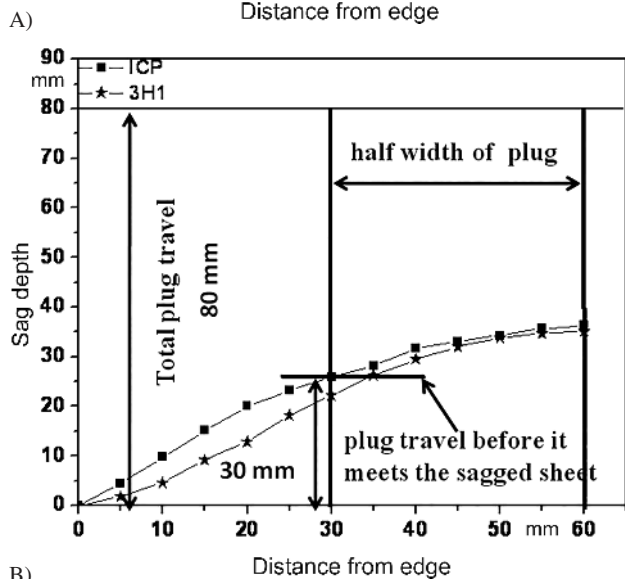
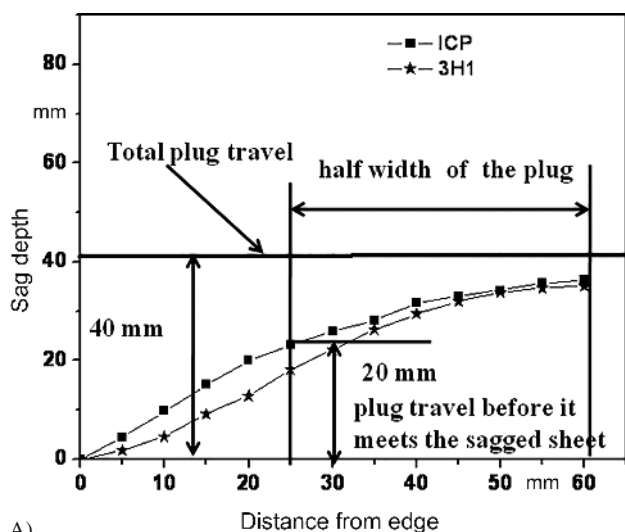


Fig. 9. Sag at the instant the plug touches the sheet for ICP and ICP-C for A) 60 mm depth cups and B) 100 mm depth cups

As an example, we compare first the 100 mm deep cups made from ICP-C and ICP materials by plug-only and PAF experiments. Figures 10A, B show representative pictures of cups made from ICP-C by plug-only forming and PAF. Since the ICP-C sheet does not sag, the plug base comes in full contact with the sheet as it starts moving down. Due to minimal slip between the sheet and the plug base, the sheet sticks to the base without any appreciable deformation during further plug travel. This is clearly seen in Fig. 10A where the circles at the base show very little deformation. The sheet forming the upper sidewall region of the component (about 0 to 20 mm arc length, zero being the point of clamping and 80 mm being the corner of the base) never comes in contact with the plug and undergoes unidirectional free stretching as can be seen in Fig. 10A from the stretching of circles into ellipses along the stretch direction. As the plug moves down further, the sheet turns along the plug corner and wraps around the plug over an arc length of 20 to 80 mm along the lower sidewall region. During this process of wrapping, the sheet necks and experiences further unidirectional increase in surface area. This is seen in Fig. 10A along the lower sidewall region where the circles have been deformed into significantly large ellipses. Upon application of vacuum after the plug motion is complete, the component experiences additional biaxial strain in the base and lower sidewall regions. As can be seen from Fig. 10B, the ellipses along the sidewalls and the circles along the base increase in size biaxially.

Figure 11A shows a comparison of thickness distribution between the ICP and ICP-C for “plug-only” experiments, and Fig. 11B shows the same for the PAF experiments. As mentioned earlier, the ICP-C sheet touches the plug base at the instant the plug begins its downward movement. Due to minimal slip between the sheet and plug base, the thickness at the base remains close to the initial thickness, i.e. 3 mm. In the case of ICP, the plug touches the sheet only after initial 30 mm travel (Fig. 9B). During this time the sheet has already thinned slightly due to the initial sag. The reduced thickness is retained in the base region during the “plug-only” experiment because of minimal slip between the sheet and the plug base. With further plug descent, the sheet thins down as it begins to wrap

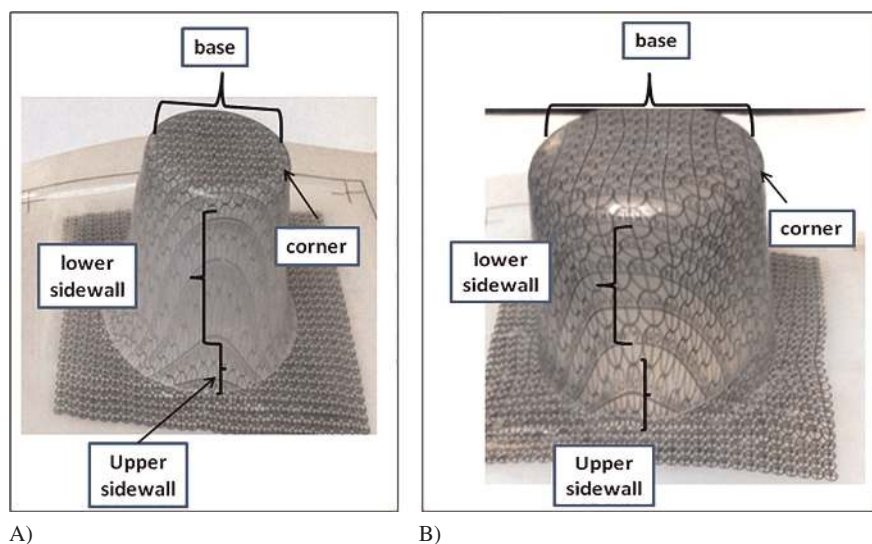


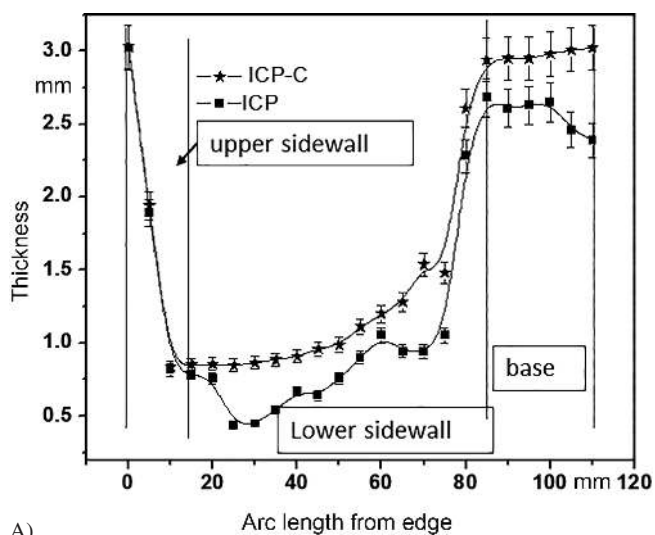
Fig. 10. Representative components, A) plug-only for ICP-C, B) fully formed component for ICP-C

around the plug in the lower sidewall region. It is seen that the thickness is lowest at the point where the sheet leaves the plug in the region between 20 and 30 mm arc length. The mechanism of deformation for both the linear ICP and branched ICP-C is similar; the difference is in the magnitude of the thickness. The difference in thickness between ICP and ICP-C is only marginal in the free stretching region while it is considerable in the lower sidewall and base regions. Figure 11B shows a comparison of thickness distribution for fully formed (PAF) components. The qualitative features of the differences between the ICP and ICP-C PAF components remain unchanged; the thickness reduces further because of the additional deformation caused by vacuum forming.

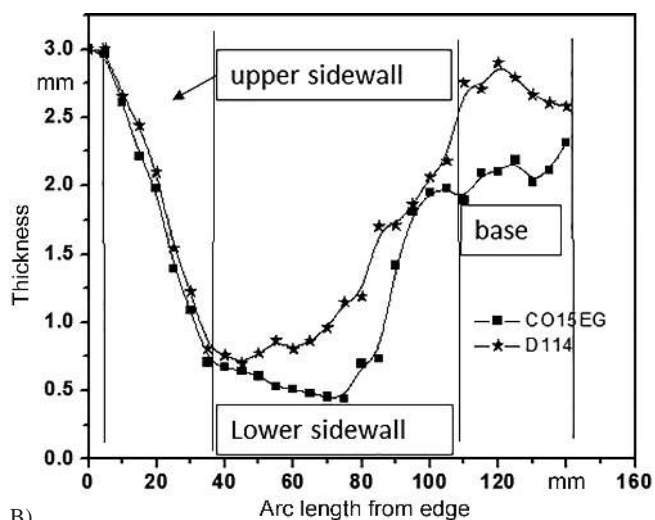
Area strain, as defined earlier, is a measure of the increase in the surface area and hence of biaxial stretching of the sheet

during forming. Since for an incompressible material like a polymer melt the trace of the strain tensor should be zero, therefore higher area strain will correspond to greater thickness reduction. The spatial distributions of area strain and thickness of PAF components made from ICP and ICP-C are seen in Fig. 12. For both polymers, the area strain is seen increasing along the upper sidewall where the sheet undergoes free stretching up to 20 mm arc length while the thickness goes on decreasing. The area strain peaks in the lower sidewall region from arc length of 20 mm to 30 mm, which coincides with the region where the sheet leaves the plug. The area strain gradually decreases further along the lower sidewall and is lowest at the base. The thickness follows the opposite behavior. It decreases along the upper sidewall, reaches a minimum in the lower side wall where the strain is the highest, and then increases along the base. Between ICP and ICP-C, the area strain is lower for the ICP-C and its corresponding thickness is higher. This is a result of the initial deformation of ICP caused by sagging and also the resistance to stretching offered by the branched ICP-C due to its extensional strain hardening nature.

Surface strains along axis-2 and axis-1 are seen in Figs. 13A, B for the 100 mm deep PAF cups of ICP and ICP-C. The geometry dictates that the surface strain along axis-2 must be greater than that along axis-1. Surface strains along both axes show similar trend as the area strain. The surface strain along axis-2 increases along the sidewall region and peaks between 50 mm to 60 mm arc length for both ICP and ICP-C. Surface strain along axis-1 also shows a similar trend for both polymers. While the surface strains along axis-2 for both ICP C and ICP are very close to each other at the base, surface strain along axis-1 is greater at the base for ICP, which is in agreement with the lower thickness at the base for ICP. Also, surface strains along the sidewall are consistently lower for ICP-C than for ICP. Though the trend in variation of surface strains is sim-



A)



B)

Fig. 11. Thickness distribution for 100 mm depth cups made from ICP and ICP-C using A) plug-only, B) PAF experiments. Error bars were obtained from statistical analysis of four cups. The different regions of the cups such as base, corner, lower side wall and upper side wall are delineated with vertical dashed lines

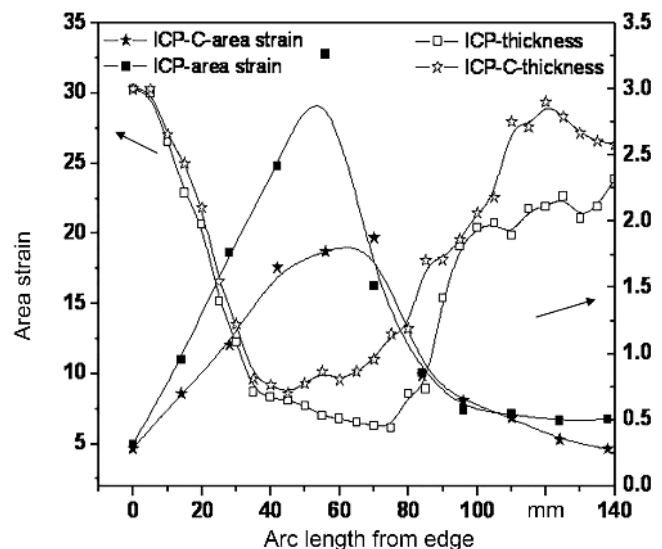
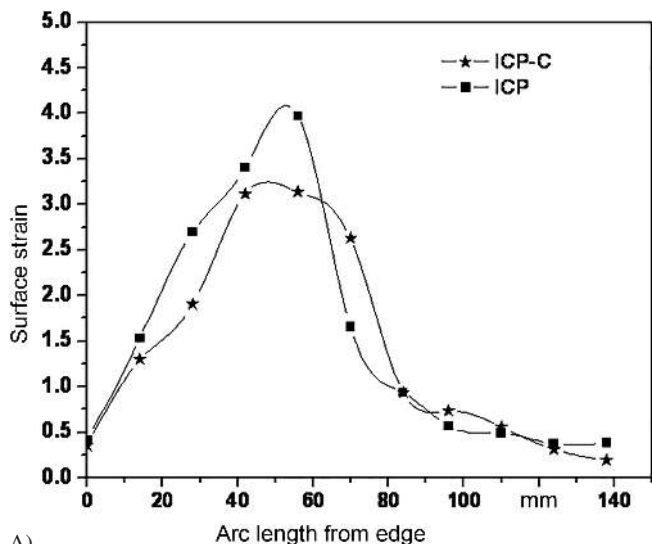


Fig. 12. Comparison of area strains and thickness distribution for 100 mm depth PAF cups made from ICP and ICP-C

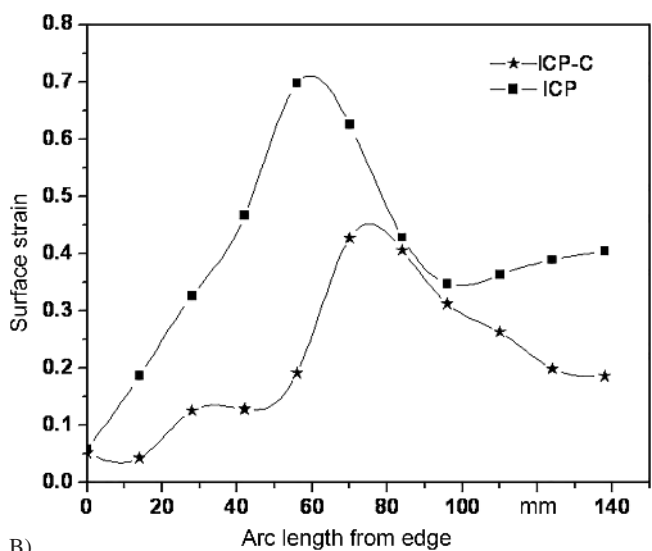
ilar for both polymers, the already thin and partially biaxially stretched sheet of ICP due to sag thins down further during the plugging and vacuum stages leading to higher surface strain and lower thickness along both axes.

We now look at results for linear and branched homopolymers 3H1 and 3H4 for the same 100 mm deep component. Figures 14A, B show the thickness distribution for “plug-only” and PAF experiments for these two polymers while Figs. 15A, B show the surface strain distributions along axes 1 and 2. These results are similar to those discussed earlier for ICP and ICP-C linear and branched copolymers. As can be seen from Fig. 14A, in “plug-only” experiments the difference in thickness between 3H1 and 3H4 is only marginal in the free stretching region (upper sidewall) while the differ-

ences in the lower sidewall and base region are considerable. Higher initial sag for 3H1 compared to 3H4 leads to lower thickness of the former. Figure 14B shows a comparison of thickness distribution for fully formed components. The difference in thickness distribution between “plug-only” and PAF is due to further thinning of the sheet on application of vacuum. Surface strain along axis-2 is higher than that along axis-1 as dictated by the geometry (Figs. 15A, B). Similar to ICP-C and ICP, while the surface strains along axis-2 for both 3H1 and 3H4 are very close to each other at the base, surface strain along axis-1 is greater at the base for 3H1 which is in agreement with the lower thickness at base for 3H1. The trends in variation of surface strains are similar for both polymers although 3H4 shows consistently lower surface strain.

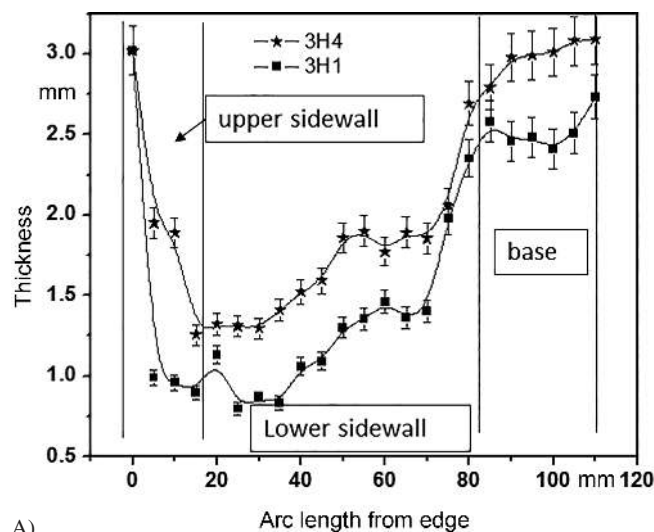


A)

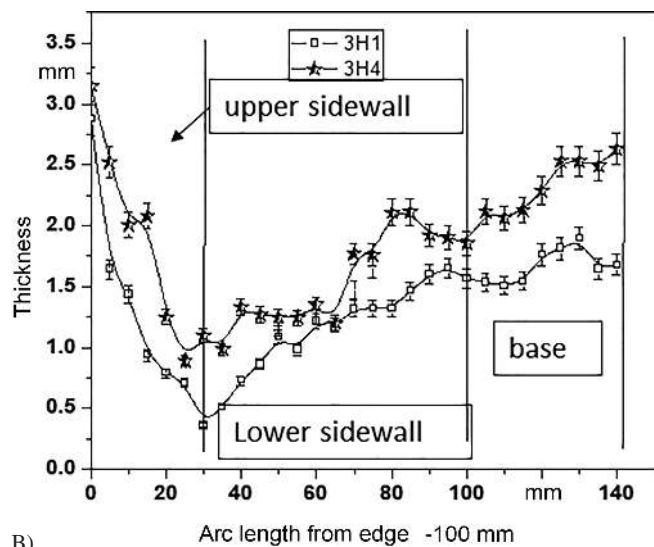


B)

Fig. 13. Surface strains for 100 mm depth PAF cups made from ICP and ICP-C along A) axis-2 and B) axis-1



A)



B)

Fig. 14. Thickness distribution for 100 mm depth cups made from 3H1 and 3H4 using A) plug-only, B) PAF experiments. Error bars were obtained from statistical analysis of four cups. The different regions of the cups such as base, corner, lower side wall and upper side wall are delineated with vertical dashed lines

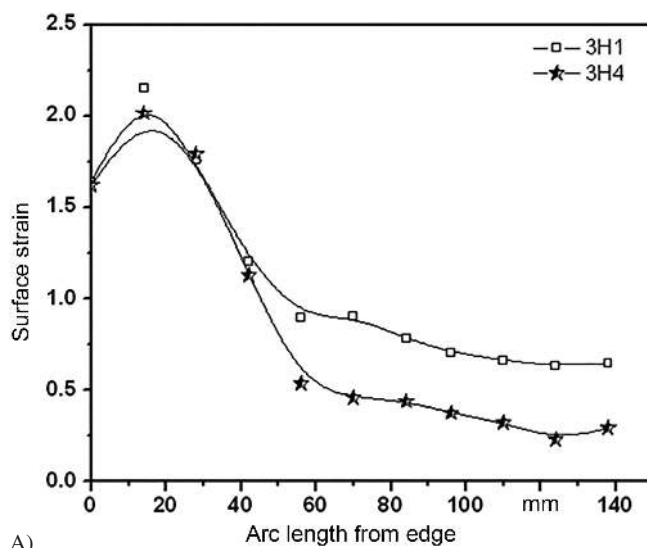
The already thin and partially biaxially stretched 3H1 sheet due to initial sag thins down further during the plugging and vacuum stage leading to higher surface strain and lower thickness along both axes.

Figures 16A, B show a comparison of aspect ratios of the deformed grid for the 100 mm deep PAF components of the linear and branched copolymers and homopolymers. A ratio of unity indicates equibiaxial stretch, a ratio  $> 1.0$  indicates a tendency to stretch uniaxially along axis-2 and a ratio  $< 1.0$  indicates a tendency to stretch uniaxially along axis-1. Figure 12A shows that for both ICP and ICP-C, the aspect ratio is greater than 1 along the sidewall indicating greater uniaxial stretching along axis-2. The ratio decreases to one at the base indicating equibiaxial stretching. Uniaxial stretching along axis-2 is higher for the branched ICP-C as compared to linear ICP. This is due to the fact that the relaxation time for the branched polymer is lar-

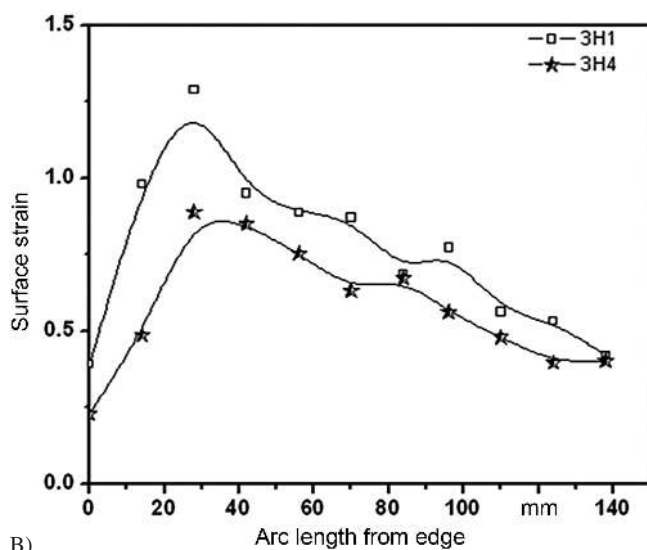
ger and so strain relaxation does not happen rapidly. For the homopolymers, the trend is similar to the copolymers except that the extent of uniaxial stretching along axis-2 is lower.

We now briefly discuss the results of thickness and surface strain distributions for the 60 mm deep cups made from linear and branched PP. Figures 17A, B show results for thickness distribution for “plug-only” and PAF experiments for the 60 mm deep cups made from ICP and ICP-C. For these cups of lower draw ratio, the plug travel is 50% of the cup depth as compared to 37% for the 100 mm deep cups. Thus, the sag effect is predominant during forming of the 60 mm deep cup. As a result, the thickness distribution of cups made from ICP-C, which does not sag, is more uniform compared to cups made from ICP, which sags to a relatively greater extent.

Figures 17C, D show surface strain along axes 1 and 2. As seen, the surface strain for the linear ICP is greater than that of

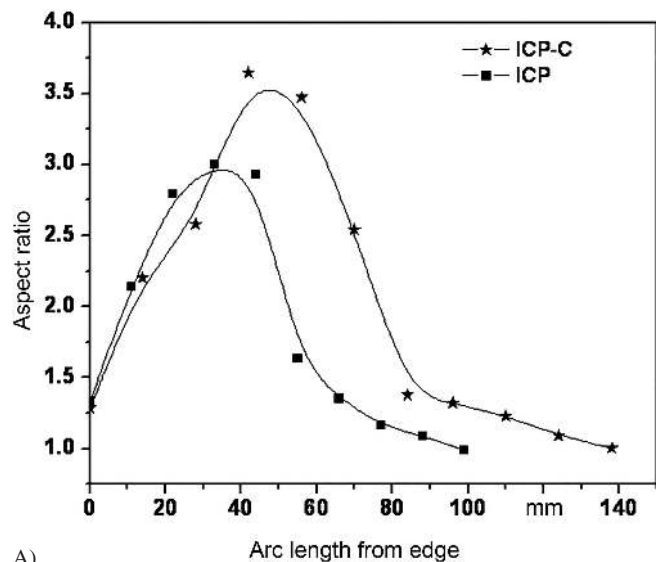


A)

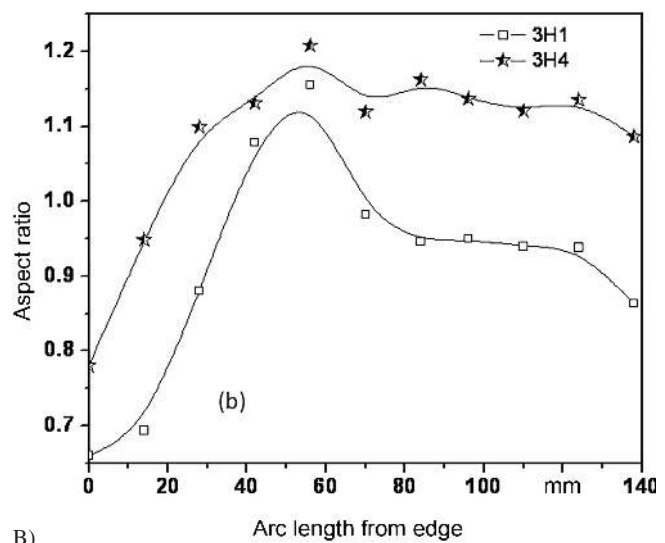


B)

Fig. 15. Surface strains for 100 mm depth PAF cups made from 3H1 and 3H4 along A) axis-2 and B) axis-1



A)



B)

Fig. 16. Aspect ratios for 100 mm depth cups for A) ICP and ICP-C and B) 3H1 and 3H4

the branched ICP-C along both axes due to higher initial sag of the ICP. For the fully formed cup, the strain along axis-1 is only marginally greater than that along axis-2. This is because of the fact that the sheet has to stretch almost the same amount circumferentially (along the axis-1) and axially (along the axis-2) because of the lower draw ratio of the cavity. This leads to near equibiaxial drawing and an aspect ratio close to 1. Though surface strains along axis-2 of the base of ICP and ICP-C are nearly the same, greater surface strain along axis-1 for linear ICP in the base region explains its lower base thickness. The trends for the homopolymers 3H1 and 3H4 are similar to the copolymers, and are therefore not discussed here in more detail.

Thus, it is seen that the strain is dictated by plug motion while the material properties contribute to sag. Extensional results show strain hardening for the branched polymers ICP-C and

3H4 whereas the linear counterparts ICP-C and 3H1 do not show any strain hardening. Since strain hardening dictates the extent of sag, ICP-C and 3H4 sag to much smaller extents than ICP and 3H1. Since the two branched polymers showed negligible sag, the plug was in complete contact with the sheet from the beginning of its stroke downwards. Thus, the strain imposed by the plug is greater for the branched polymers than for the linear polymers. Table 3 summarizes the results of all the experiments.

#### 4 Conclusions

Plug assist thermoforming (PAF) and “plug-only” forming experiments were carried out for linear and long chain branched PP homopolymers and impact copolymers at temperatures be-

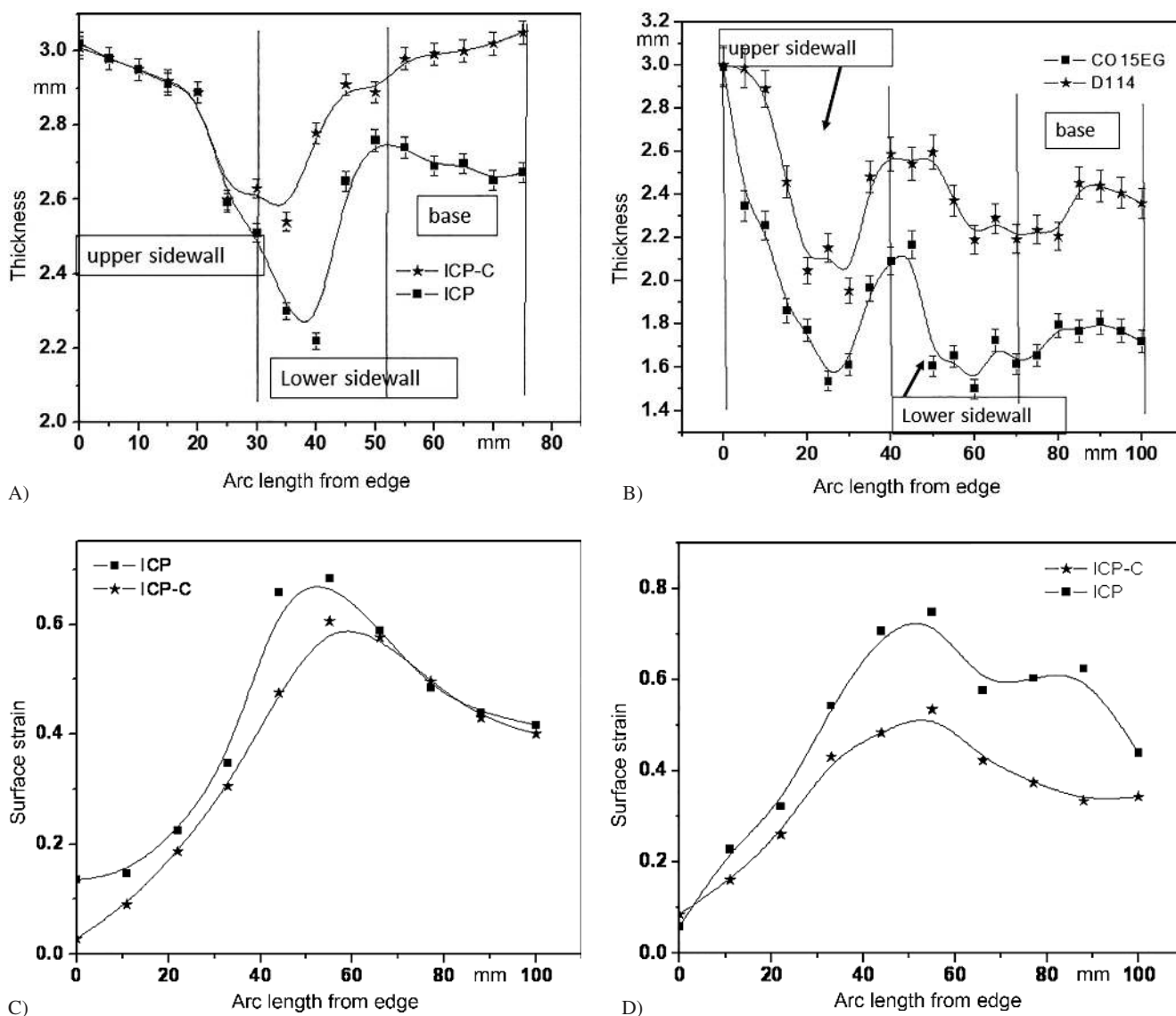


Fig. 17. Thickness distribution for 60 mm depth cups made from ICP and ICP-C using A) plug-only, B) PAF experiments. Error bars were obtained from statistical analysis of four cups. The different regions of the cups such as base, corner, lower side wall and upper side wall are delineated with vertical dashed lines. Surface strains for 60 mm depth PAF cups made from ICP and ICP-C along C) axis-2 and D) axis-1

yond the peak melting temperatures of the polymers. Axisymmetric cup-shaped cavities of two depths – 100 mm and 60 mm, and their corresponding plugs were used for forming. A detailed understanding of the deformation mechanism of the sheets during forming was attempted by measuring surface strain distributions and thickness distributions. An attempt was

also made to qualitatively relate the observed surface strain and thickness distributions with the rheological properties of the linear and branched polymers.

Experimental results showed conclusively that the type and the extent of deformation are influenced by the draw depth and the rheological properties of the polymer; the latter con-

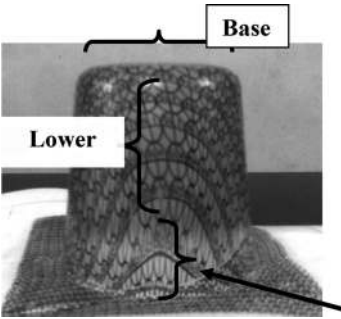
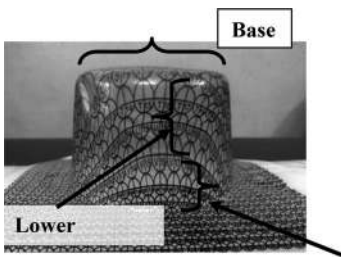
	100 mm Depth cup	60 mm Depth cup
		
Figures	<ul style="list-style-type: none"> <li>• Figures 11A, B and Figs. 14A, B show thickness distribution for branched and linear copolymers and homopolymers, respectively</li> <li>• Figures 13A, B and Figs. 15A, B show surface strain distribution for branched and linear copolymers and homopolymers, respectively</li> <li>• Figures 16A, B show aspect ratio for branched and linear copolymers and homopolymers, respectively.</li> </ul>	<ul style="list-style-type: none"> <li>• Figures 17A, B show thickness distribution for branched and linear copolymers and homopolymers, respectively</li> <li>• Figures 17C, D show surface strain distribution for branched and linear copolymers and homopolymers respectively.</li> </ul>
Upper sidewall region	<ul style="list-style-type: none"> <li>• Free unconstrained stretching between 0 to 30 mm arc length for both linear and branched polymers during the plugging stage.</li> <li>• Differences between linear and branched PP in terms of surface strain and thickness of fully formed cups are marginal (Figs. 11A, B).</li> <li>• Aspect ratio between 2 and 2.5 for both branched and linear PP indicating uniaxial stretching along axis-2.</li> <li>• Only marginal difference in thickness distribution and surface strain for cups made from linear and branched polymers.</li> </ul>	<ul style="list-style-type: none"> <li>• Free unconstrained stretching between 0 to 35 mm arc length for both linear and branched polymers during the plugging stage.</li> <li>• Significant differences between linear and branched PP in terms of surface strains and thickness of fully formed cups; thickness for branched PP is higher by around 20% due to initial sag for linear materials.</li> <li>• Aspect ratio is around 1 for both linear and branched polymers indicating equiaxial stretching.</li> </ul>
Lower sidewall region	<ul style="list-style-type: none"> <li>• Sheet thinning due to wrapping around plug during plugging stage; thinnest in the region where sheet leaves plug (between 20 mm to 30 mm arc length in “plug-only” experiments).</li> <li>• Differences between linear and branched polymers with regards to surface strain and thickness; these are greater compared to upper sidewall since forming in lower sidewall is influenced by plug action, while that in the upper sidewall is free unconstrained forming.</li> <li>• Aspect ratio between 3 to 3.5 for branched and 2.5 to 3 for linear polymers indicating uniaxial stretching to greater extent than upper sidewall for fully formed cups.</li> <li>• Only marginal difference in thickness distribution and surface strain for cups made from linear and branched polymers.</li> </ul>	<ul style="list-style-type: none"> <li>• Sheet thinning due to wrapping around plug; thinnest in the region where sheet leaves plug (between 25 mm to 30 mm) during the plugging stage.</li> <li>• Significant differences in surface strain and thickness for linear and branched polymers (thickness for branched greater by about 20%).</li> <li>• Aspect ratio is around 1 for both linear and branched polymers indicating equiaxial stretching.</li> </ul>

Table 3. continued on next page

Base region	<ul style="list-style-type: none"> <li>• For branched polymers, sheet touches plug base immediately as the plug starts moving. Sheet touches plug base after 27 mm travel for the linear polymer. Due to this, base thickness for cups made from a branched polymer is higher.</li> <li>• Aspect ratio close to one for both the polymers indicating equibiaxial stretching for fully formed cups.</li> <li>• Minimal slip, so base thicker than sidewall for both linear and branched.</li> <li>• Base thickness for the branched polymer is higher by about 20 % than that for linear polymer for fully formed cups.</li> <li>• Only marginal difference in thickness distribution and surface strain for cups made from linear and branched polymers.</li> </ul>	<ul style="list-style-type: none"> <li>• Sheet touches plug base instantaneously for branched polymer. Sheet touches plug base after 20 mm travel for linear polymer. Due to this, the base thickness for cups made from branched polymer is higher.</li> <li>• Aspect ratio is around 1 for both linear and branched polymers indicating equiaxial stretching.</li> <li>• Minimal slip, so base thicker than sidewall for both linear and branched polymers.</li> <li>• Average base thickness for branched polymer is higher by about 25 % than that for linear polymer.</li> </ul>
Salient conclusions	<i>The nature of deformation during forming and the extent of deformation are influenced to a greater extent by draw ratio than material properties.</i>	<i>The nature of deformation during forming is influenced by draw ratio whereas the extent of deformation is influenced predominantly by material properties.</i>

Table 3. Summary of comparative results for thermoformed cups of 100 mm and 60 mm depth made from linear and branched PP samples

trols the resistance to deformation as well as the initial sag before forming begins. Thus, while the type of deformation of the base regions of all cups remained equibiaxial, the type of deformation in the sidewall regions of the cup changed from predominantly uniaxial to more equibiaxial as the draw depth decreased from 100 mm to 60 mm. Components formed using branched polymers possessed greater average thickness and lower surface strains as compared to those formed using linear polymers for the same mold and plug geometry.

It was found that sag behavior of linear and branched PP sheets has a subtle effect on the surface strain distribution and thickness distribution. Independent isothermal sag experiments showed that branched PP showed relatively negligible sag prior to forming as compared to linear PP. This was due to the higher zero shear viscosity, higher melt elasticity and melt strength of the branched polymers. The lower sag of branched PP sheets prior to forming ensured that the deformation occurred primarily by the plug forming step followed to a smaller extent by the vacuum forming step. In contrast, higher sag of linear PP sheets prior to forming meant that the sheets were already biaxially stretched to some extent before they were deformed by plug forming and subsequent vacuum forming. Thus, the influence of the plug forming step was relatively lower for the linear PP compared to the branched PP. As a result, the area strain and circumferential surface strain were higher for the linear PP cups compared to the branched PP cups. Correspondingly, the thickness of the linear PP cups was lower.

## References

- Arnold, M., Bornemann, S., Schimmel, T. and Heinze, T., "Modified Polypropylenes by Copolymerization with Nonconjugated Dienes and Additional Chemical Reactions", *Macromol. Symp.*, **181**, 5–16 (2002)
- Barroso, V. C., Ribeiro, S. P. and Maia, J. M., "Unusual Extensional Behavior of A Polystyrene/HIPS Blend", *Rheol. Acta*, **42**, 483–490 (2003), DOI:10.1007/s00397-003-0303-1
- Bettini, S. H. P., Agnelli, J. A. M., "Grafting of Maleic Anhydride onto Polypropylene by Reactive Extrusion", *J. Appl. Polym. Sci.*, **85**, 2706–2717 (2002), DOI:10.1002/app.10705
- Borsig, E., Fiedlerova, A., Rychla, L., Lazar, M., Ratzsch, M. and Haudel, G., "Crosslinking of Polypropylene-Polyethylene Blends by Peroxide and the Effect of Pentaerythritol Tetraallyl Ether", *J. Appl. Polym. Sci.*, **37**, 467–478 (1989), DOI:10.1002/app.1989.070370213
- Chikhalikar, K., Banik, S., Azad, L., Jadhav, K., Mahajan, S., Ahmad, Z., Kulkarni, S., Gupta, S., Doshi, P. and Lele, A., "Extrusion Film Casting of Long Chain Branched Polypropylene", *Polym. Eng. Sci.*, **55**, 1977–1987b (2015), DOI:10.1002/pen.24039
- Chodak, I., Lazar, M., "Effect of the Type of Radical Initiator on Crosslinking of Polypropylene", *Angew. Makromol. Chem.*, **106**, 153–160 (1982), DOI:10.1002/apmc.1982.051060111
- Coiai, S., Passaglia, E., Aglietto, M. and Ciardelli, F., "Control of Degradation Reactions during Radical Functionalization of Polypropylene in the Melt", *Macromolecules*, **37**, 8414–8423 (2004), DOI:10.1021/ma0400315
- Denicola, A. J., U.S. Patent 5047485A (1990)
- Graebing, D., "Synthesis of Branched Polypropylene by a Reactive Extrusion Process", *Macromolecules*, **35**, 4602–4610 (2002), DOI:10.1021/ma0109469
- Gezaz, S.-M., Ghasemi, I., Karrabi, M. and Azizi, H., "Investigation on the Thermoformability of Polyolefin Blends by Hot Tensile and Rheological Tests," *Polym. Test.*, **25**, 504–511 (2006), DOI:10.1016/j.polymertesting.2006.02.002
- Gotsis, A. D., Zeevenhoven, B. L. F. and Hogt, A. H., "The Effect of Long Chain Branching on the Processability of Polypropylene in Thermoforming", *Polym. Eng. Sci.*, **44**, 973–982 (2004), DOI:10.1002/pen.20089
- Guo, P., Xu, Y., Lu, M. and Zhang, S., "High Melt Strength Polypropylene with Wide Molecular Weight Distribution Used as Basic Resin for Expanded Polypropylene Beads", *Ind. Eng. Chem. Res.*, **54**, 217–225 (2014), DOI:10.1021/ie503503k
- Kasehagen, L. J., Macosko, C. W., Trowbridge, D. and Magnus, F., "Rheology of Long Chain Randomly Branched Polybutadiene", *J. Rheol.*, **40**, 689–709 (1996), DOI:10.1122/1.550732
- Kim, B. K., Kim, K. J., "Cross-Linking of Polypropylene by Peroxide and Multifunctional Monomer during Reactive Extrusion", *Adv. Polym. Technol.*, **12**, 263–269 (1993), DOI:10.1002/adv.1993.060120304



- Kumar Shyam, P., Kumar, K. G., Kommoji, S., Banerjee, R. and Ghosh, A. K., "The Effect of Material Characteristics and Mould Parameters on the Thermoforming of Thick Polypropylene Sheets", *J. Plast. Film Sheeting*, **30**, 162–181 (2014)
- Lagendijk, R. P., Hogt, A. H., Buijtenhijns, A. and Gotsis, A. D., "Peroxycarbonate Modification of Polypropylene and Extensional Flow Properties", *Polymer*, **42**, 1003510043 (2001), DOI:10.1016/S0032-3861(01)00553-5
- Lau, H. C., Bhattacharya, S. N. and Field, G. J., "Melt Strength of Polypropylene: Its Relevance to Thermoforming", *Polym. Eng. Sci.*, **38**, 1915–1923 (1998), DOI:10.1002/pen.10362
- Lau, H. C., Bhattacharya, S. N. and Field, G. J., "Influence of Rheological Properties on the Sagging of Polypropylene and ABS Sheet for Thermoforming Applications" *Polym. Eng. Sci.*, **40**, 1564–1570 (2000), DOI:10.1002/pen.11286
- Maier C., Calafut T., "Polypropylene: The Definitive User's Guide and Databook", *Plastic Design Library*, 1–8 and 260–275 (1998)
- Mabrouk, K., Parent, J. S., Chaudhary, B. I. and Cong, R., "Chemical Modification of PP Architecture: Strategies for Introducing Long-Chain Branching", *Polymer*, **50**, 5390–5397 (2009), DOI:10.1016/j.polymer.2009.09.066
- Martin, P. J., Tan, C. W., Tshai, K. Y., Mccool, R., Menary, G., Armstrong C. G. and Harkin- Jones, E. M. A., "Biaxial Characterisation of Materials for Thermoforming and Blow Moulding", *Plast. Rubber Compos.*, **34**, 276–282 (2005), DOI:10.1179/174328905X64803
- Moad, G., "The Synthesis of Polyolefin Graft Copolymers by Reactive Extrusion", *Prog. Polym. Sci.*, **24**, 81–142 (1999), DOI:10.1016/S0079-6700(98)00017-3
- McCool, R., Martin P., "The Role of Process Parameters in Determining Wall Thickness Distribution in Plug-Assisted Thermoforming", *Polym. Eng. Sci.*, **50**, 19231934 (2010), DOI:10.1002/pen.21718
- Munstedt, H., Kurzbeck, S. and Stange, J., "Importance of Elongational Properties of Polymer Melts for Film Blowing and Thermoforming", *Polym. Eng. Sci.*, **46**, 1190–1195 (2006)
- O'Connora, C. P. J., Menary, G., Martin, P. J. and Mcconville, E., "Finite Element Analysis of the Thermoforming of Polypropylene", *Int. J. Mat. Forming*, **1**, 779–782 (2008)
- Park, C. B., Cheung, L. K., "A Study of Cell Nucleation in the Extrusion of Polypropylene Foams", *Poly. Eng. Sci.*, **37**, 1–10 (1997), DOI:10.1002/pen.11639
- Parent, J., Sengupta, S., Kaufman M. and Chaudhary, B. I., "Coagent-Induced Transformations of Polypropylene Microstructure: Evolution of Bimodal Architectures and Cross-Linked Nano-Particles", *Polymer*, **49**, 3884–3891 (2008), DOI:10.1016/j.polymer.2008.07.007
- Parent, J. S., Bodsworth, A., Sengupta, S. S., Kontopoulou, M., Chaudhary, B. I., Poche, D. and Cousteaux, S., "Structure–Rheology Relationships of Long-Chain Branched Polypropylene: Comparative Analysis of Acrylic and Allylic Coagent Chemistry", *Polymer*, **50**, 85–94 (2009), DOI:10.1016/j.polymer.2008.11.014
- Pol, H. V., Joshi, Y. M., Tapadia, P. S., Lele, A. K. and Mashelkar, R. A., "A Geometrical Solution to the Sharkskin Instability", *Ind. Eng. Chem. Res.*, **46**, 3048–3056 (2007), DOI:10.1021/ie0610391
- Scheve, B. J., Mayfield, J. W. and Denicola Jr., A. J., U.S. Patent No. 4 916 198 (1990)
- Schaeffler, D. J., Vineberg, E. J., "Chapter 66 Troubleshooting Formability Problems Using Strain Analysis, in ASM Handbook, Metalworking: Sheet Forming, The Materials Information Society, Ohio, USA, p. 697–706 (2006)
- Sowerby, R., Chu, E. and Duncan, J., "Determination of Large Strains in Metal Forming", *J. Strain Anal. Eng. Des.*, **17**, 95–101 (1982), DOI:10.1243/03093247V172095
- Spitael, P., Macosko, C. W., "Strain Hardening in Polypropylenes and its Role in Extrusion Foaming", *Polym. Eng. Sci.*, **44**, 2090–2100 (2004), DOI:10.1002/pen.20214
- Shiono, T., Azad, S. M. and Ikeda, T., "Copolymerization of Atactic Polypropene Macromonomer with Propene by an Isospecific Metallocene Catalyst", *Macromolecules*, **32**, 5723–5727 (1999), DOI:10.1021/ma9903963
- Su, F. H., Huang, H. X., "Rheology and Melt Strength of Long Chain Branching Polypropylene Prepared by Reactive Extrusion with Various Peroxides", *Polym. Eng. Sci.*, **50**, 342–351 (2010), DOI:10.1002/pen.21544
- Throne, J. L.: *Technology of Thermoforming*, 1<sup>st</sup> Edition, Hanser/Gardner Publications, Cincinnati (1996), PMID:8672655; DOI:10.3139/9783446402478
- Throne, J. L., "Advances in Thermoforming", *Rapra Review Reports*, **8**, 3–4 (1997)
- Tripathi, D.: *Practical Guide to Polypropylene*, Rapra Technology, Shrewberry (2002)
- Tzoganakis, C., Vlachopoulos, J. and Hamielec, A. E., "Production of Controlled Rheology Polypropylene Resins by Peroxide Promoted Degradation during Extrusion", *Polym. Eng. Sci.*, **28**, 170–180 (1988), DOI:10.1002/pen.760280308
- Wagner, M. H., "A Constitutive Analysis of Uniaxial Elongational Flow Data of Low-Density Polyethylene Melt", *J. Non-Newtonian Fluid Mech.*, **4**, 39–55 (1978), DOI:10.1016/0377-0257(78)85005-8
- Wang, X., Tzoganakis, C. and Rempel, G. L., "Chemical Modification of Polypropylene with Peroxide/Pentaerythritol Triacrylate by Reactive Extrusion," *J. Appl. Polym. Sci.*, **61**, 1395–1404 (1996), DOI:10.1002/(SICI)1097-4628(19960822)61:8<1395::AID-APP21>3.0.CO;2-X

## Acknowledgements

The authors would like to thank Dr. Pramod Joshi, Ex-Head Polymer Engineering Department, MIT, Pune for making available the thermoforming machine for this research.

*Date received: April 26, 2018*

*Date accepted: December 20, 2018*

Bibliography  
DOI 10.3139/217.3704  
Intern. Polymer Processing  
XXXIV (2019) 3; page 339–355  
© Carl Hanser Verlag GmbH & Co. KG  
ISSN 0930-777X